PLANE-WAVE REFLECTION FROM INHOMOGENEOUS UNIAXIALLY ANISOTROPIC ABSORBING DIELECTRIC LAYERS

by
Edward F. Kuester and Christopher L. Holloway

Electromagnetics Laboratory
Department of Electrical and Computer Engineering
Campus Box 425
University of Colorado
Boulder, Colorado 80309-0425

May 1989

Abstract

In previous work, it has been shown that the low-frequency behavior of a periodic array of absorbing wedges or pyramid cones is equivalent to that of a layered anisotropic absorbing medium whose effective permittivity and permeability depend on those of the absorber and the geometry of the structure. In this report, we study the reflection of plane waves from this equivalent layered medium for the purpose of understanding and improving the performance of such absorber arrays in the frequency range of 30-300 MHz. By modifying some existing types of standard absorber, we are able to come up with improved designs that should find important application in the lining of anechoic measurement chambers for the frequency range of 30-1000 MHz.

1 Introduction

Anechoic electromagnetic measurement chambers are frequently lined with pyramid cone absorbers which serve as gradual, low-reflection coverings for the metallic shielding walls on the outside of the room. Extensive summaries of the principles and design of such chambers are to be found in [1]-[4]. At sufficiently low frequencies that the height of the cones (i. e. , the thickness of the absorber wall covering) is no longer large compared to wavelength and skin depth in the absorbing medium, the performance of the absorber will deteriorate as compared to higher frequencies. In [5] it was demonstrated that at sufficiently low frequencies (periods of the cones small compared to a wavelength) a gently tapered absorber array behaves as a one-dimensionally inhomogeneous but anisotropic medium, as far as the "average" field is concerned. The equivalent permittivity and permeability for this structure are obtained from the solution of the *static* field problems for an array of absorbing cylinders with no taper at all. It is the purpose of this report to study the behavior of the reflection coefficient of a plane wave from this equivalent plane-layered absorbing medium.

Consider, for example, the periodic array of slabs shown in Fig.1. It has been known for some time [6]-[11] that this medium behaves like a uniaxially anisotropic but homogeneous material with (possibly complex) tensor permittivity $[\epsilon]$ and permeability $[\mu]$:

$$[\epsilon] = \begin{bmatrix} \epsilon_x & 0 & 0 \\ 0 & \epsilon_y & 0 \\ 0 & 0 & \epsilon_z \end{bmatrix} \tag{1}$$

$$[\mu] = \begin{bmatrix} \mu_x & 0 & 0 \\ 0 & \mu_y & 0 \\ 0 & 0 & \mu_z \end{bmatrix} \tag{2}$$

If the period a of this laminated medium is small compared to a wavelength in
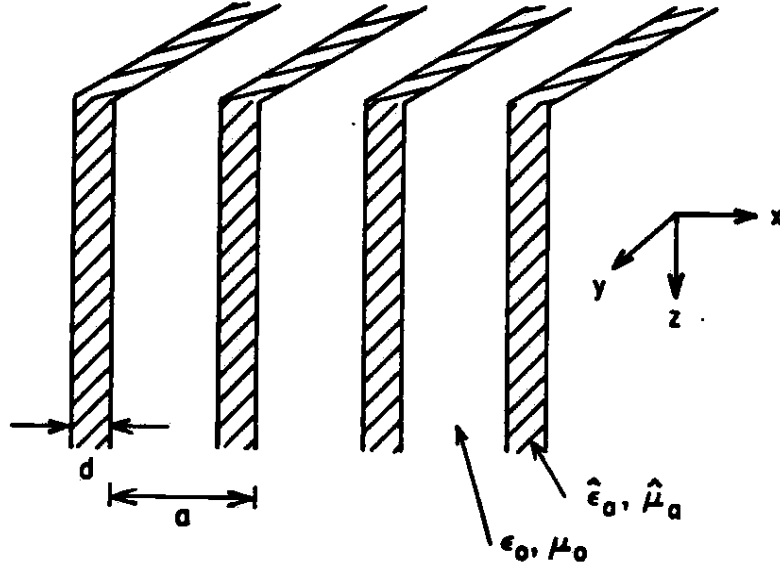
1

Figure 1: Periodic array of absorbing slabs.

either medium, as well as to the skin depth, then:

$$
\left.\begin{array}{rcl}
\epsilon_x^{-1} & = & (1-g)\epsilon_0^{-1} + g\epsilon_a^{-1} \\
\mu_x^{-1} & = & (1-g)\mu_0^{-1} + g\mu_a^{-1} \\
\epsilon_y = \epsilon_z & = & (1-g)\epsilon_0 + g\epsilon_a \\
\mu_y = \mu_z & = & (1-g)\mu_0 + g\mu_a
\end{array}\right\}
\tag{3}
$$

where $g = d/a$ is the relative volume of space occupied by the absorber, ϵ_a and μ_a are the complex parameters of the bulk absorber, and ϵ_0 and μ_0 are those of free space.

For the two-dimensional square array of square absorbing rods shown in Fig. 2 (which, when tapered, becomes the pyramid-cone absorber array), the elements μ_z and ϵ_z are known exactly [5]:

$$
\left.\begin{array}{rcl}
\epsilon_z & = & (1-g^2)\epsilon_0 + g^2\epsilon_a \\
\mu_z & = & (1-g^2)\mu_0 + g^2\mu_a
\end{array}\right\}
\tag{4}
$$

where $g = d/a$, and g^2 represents the volume fraction of space occupied by the absorber. While no exact, closed-form expression for $\epsilon_t = \epsilon_x = \epsilon_y$ and $\mu_t = \mu_x = \mu_y$ exists for this case, numerical evidence presently available suggests
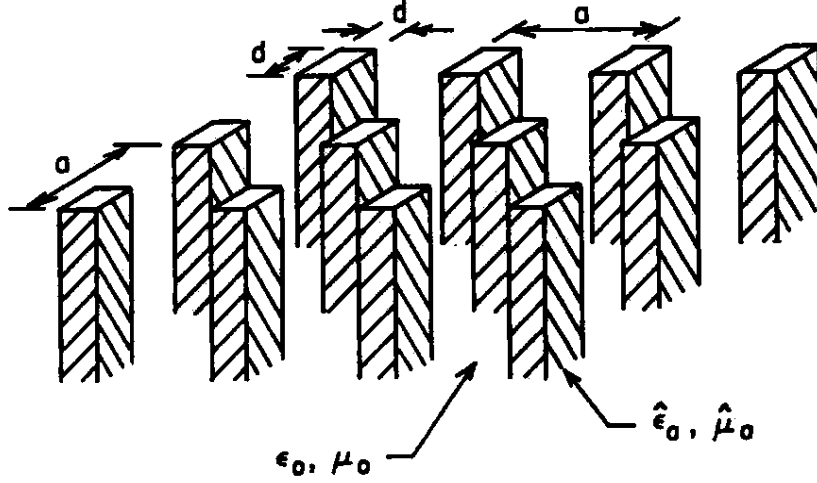
2

Figure 2: Square array of square absorbing rods.

that the Hashin-Shtrikman formulas

$$
\left.
\begin{aligned}
\epsilon_t &= \epsilon_0 \left[1 + g^2 \frac{2(\epsilon_a - \epsilon_0)}{(1+g^2)\epsilon_0 + (1-g^2)\epsilon_a} \right] \\
\mu_t &= \mu_0 \left[1 + g^2 \frac{2(\mu_a - \mu_0)}{(1+g^2)\mu_0 + (1-g^2)\mu_a} \right]
\end{aligned}
\right\}
\tag{5}
$$

should be quite accurate for the values of ϵ_a, μ_a and g encountered in practice (on the order of 5 percent error [5]).

A comparison of ϵ_z with ϵ_t is plotted in Fig. 3 for the case of $\epsilon_a = 10\epsilon_0$, using eqn. (5). The degree of anisotropy of the equivalent homogeneous medium is seen to be quite pronounced when ϵ_a/ϵ_0 is this large, unless g is very close to 0 or 1 (bulk air or bulk absorber limits, respectively). It is to be expected that this anisotropy may significantly affect the propagation of plane waves in this medium at oblique angles to the axes of the rods.

If the widths of the layers or rods in Figs. 1 or 2 vary with z as shown in Fig. 4, we have shown in [5] that the resulting array of wedges or pyramid cones is equivalent to an *inhomogeneous* anisotropic absorbing layer with effective parameters $[\epsilon(z)]$ and $[\mu(z)]$ as shown in Fig. 5. These z-dependent tensors are obtained from (4) and (5) (or from (3) in the case of wedges) by letting $g \rightarrow g(z) = d(z)/a$ in these formulas. Of course, a gentle variation of the values of ϵ_a and μ_a with z would also be a way to vary $[\epsilon(z)]$ and $[\mu(z)]$, so that further flexibility in these tensor functions can be achieved if desired. At low
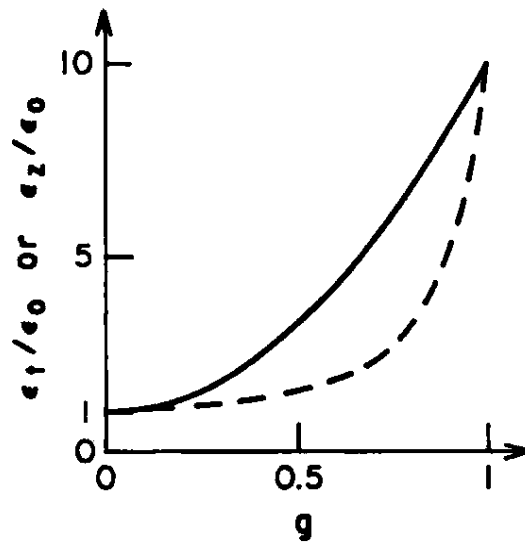
3

Figure 3: Comparison of ϵ_z and ϵ_t for $\epsilon_a = 10\epsilon_0$: ———— ϵ_z; - - - - - ϵ_t.
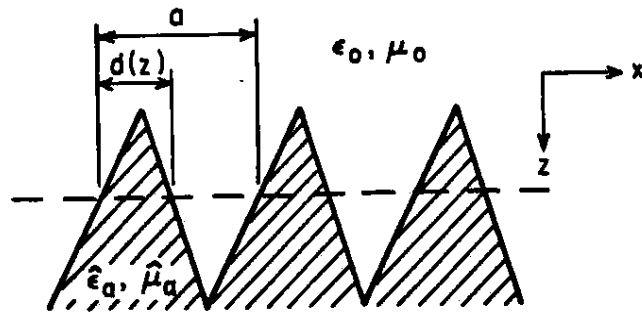

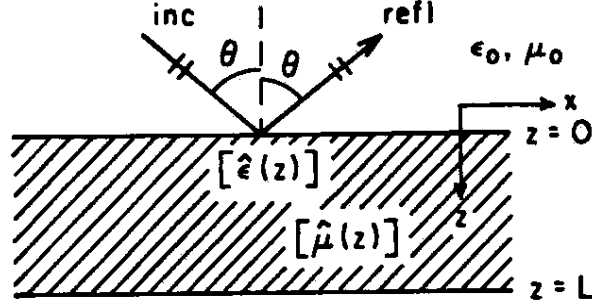Figure 4: Array of wedges or cones.

4

Figure 5: Equivalent inhomogeneous anisotropic absorbing layer.

frequencies, then, the modelling of geometrically tapered absorbers is simplified considerably into a one-dimensionally varying plane layer problem. It is this problem that we address in the present report.

2   Reflection from an Inhomogeneous Uniaxially Anisotropic Layer

Consider the problem of a plane wave in air incident at an angle θ from the normal to the inhomogeneous anisotropic layer shown in Fig. 5. Assuming that the plane of incidence is the xz-plane as shown, we may assume $\partial/\partial y \equiv 0$ for all fields which result. For a uniaxially anisotropic medium described by the tensors (1) and (2), Maxwell's equations decouple into two independent sets; one for perpendicular polarization:

$$
\left.
\begin{array}{rcl}
\frac{\partial H_x}{\partial z} - \frac{\partial H_z}{\partial x} & = & j\omega\hat{\epsilon}_y E_y \\[4pt]
\frac{\partial E_y}{\partial z} & = & -j\omega\hat{\mu}_x H_x \\[4pt]
-\frac{\partial E_y}{\partial x} & = & -j\omega\hat{\mu}_z H_z
\end{array}
\right\}
\tag{6}
$$

5

and one for parallel polarization:

$$\left.\begin{array}{rcl} \frac{\partial E_z}{\partial x} - \frac{\partial E_x}{\partial z} & = & -j\omega\hat{\mu}_y H_y \\ \frac{\partial H_y}{\partial z} & = & j\omega\hat{\epsilon}_z E_z \\ -\frac{\partial H_y}{\partial x} & = & j\omega\hat{\epsilon}_x E_x \end{array}\right\} \qquad (7)$$

where a time factor of $e^{j\omega t}$ has been assumed. Since the incident wave determines an x-dependent factor $e^{-jk_0 x \sin\theta}$ (where $k_0 = \omega\sqrt{\mu_0\epsilon_0}$) which will be common to the entire field, we can eliminate the explicit x-dependence in (6) and (7) also, as well as the z-components of the fields. The result for either polarization can be cast in the form

$$\left.\begin{array}{rcl} \frac{dE(z)}{dz} & = & -j\omega\hat{\mu}_{eff}(z)H(z) \\ \frac{dH(z)}{dz} & = & -j\omega\hat{\epsilon}_{eff}(z)E(z) \end{array}\right\} \qquad (8)$$

where for perpendicular polarization:

$$E(z) = E_y(z) \qquad\qquad H(z) = -H_x(z) \qquad (9)$$

$$\left.\begin{array}{rcl} \hat{\epsilon}_{eff}(z) & = & \hat{\epsilon}_y(z) - \frac{\mu_0\epsilon_0 \sin^2\theta}{\hat{\mu}_x(z)} \\ \hat{\mu}_{eff}(z) & = & \hat{\mu}_x(z) \end{array}\right\} \qquad (10)$$

while for parallel polarization:

$$E(z) = E_x(z) \qquad\qquad H(z) = H_y(z) \qquad (11)$$

$$\left.\begin{array}{rcl} \hat{\epsilon}_{eff}(z) & = & \hat{\epsilon}_x(z) \\ \hat{\mu}_{eff}(z) & = & \hat{\mu}_y(z) - \frac{\mu_0\epsilon_0 \sin^2\theta}{\hat{\epsilon}_z(z)} \end{array}\right\} \qquad (12)$$

Equations (8) are analogous to the classical equations for a nonhomogeneous transmission line. We therefore exploit this analogy by writing

$$\hat{Z}_c(z) = \sqrt{\frac{\hat{\mu}_{eff}(z)}{\hat{\epsilon}_{eff}(z)}} \qquad (13)$$

$$\hat{\gamma}(z) = \alpha(z) + j\beta(z) = j\omega\sqrt{\hat{\mu}_{eff}(z)\hat{\epsilon}_{eff}(z)} \qquad (14)$$

as a characteristic impedance and propagation constant, both dependent on z and known if all the layer parameters are known.

The analysis of such inhomogeneous lines is well-known [11],[12], and we follow these developments here. We define the field impedance

$$Z(z) = E(z)/H(z) \qquad (15)$$

6

for which, from (8), it is possible to obtain a Riccati equation:

$$
\begin{aligned}
Z'(z) &= -j\omega[\hat{\mu}_{eff}(z) - \hat{\epsilon}_{eff}(z)Z^2(z)] \\
&= -\hat{\gamma}(z)[\hat{Z}_c(z) - Z^2(z)/\hat{Z}_c(z)]
\end{aligned}
\tag{16}
$$

If $Z(z)$ is found, the electric field reflection coefficient for the plane wave at the surface of the inhomogeneous layer can be written as

$$
\Gamma(0) = \frac{Z(0) - \hat{Z}_c(0)}{Z(0) + \hat{Z}_c(0)}
\tag{17}
$$

in the usual way. Although there is more than one way to define a position-dependent reflection coefficient within the layer which reduces to (17) when $z = 0$ [13], we find it most convenient here to use the Schelkunoff definition:

$$
\Gamma(z) \equiv \frac{Z(z) - \hat{Z}_c(z)}{Z(z) + \hat{Z}_c(z)}; \qquad Z(z) = \hat{Z}_c(z)\frac{1 + \Gamma(z)}{1 - \Gamma(z)}
\tag{18}
$$

When this is differentiated and used with (16), we obtain a Riccati equation for $\Gamma(z)$ itself:

$$
\Gamma'(z) = 2\hat{\gamma}(z)\Gamma(z) - \hat{N}(z)[1 - \Gamma^2(z)]
\tag{19}
$$

where

$$
\hat{N}(z) \equiv \frac{\hat{Z}_c'(z)}{2\hat{Z}_c(z)}
\tag{20}
$$

is a measure of the nonuniformity of the characteristic impedance. Clearly $\hat{N} = 0$ in a homogeneous section where $\hat{Z}_c$ is constant.

When $\hat{N} \equiv 0$, the Riccati equation (19) may be solved exactly to get the well-known solution

$$
\Gamma(z) = \Gamma(0)\exp[2\int_0^z \hat{\gamma}(z')\,dz']
\tag{21}
$$

If z_0 is located at the surface of a perfect conductor, then we have the boundary condition

$$
\Gamma(z_0) = -1 \qquad \text{(perfect conductor)}
\tag{22}
$$

since $Z(z_0) = 0$. If z_0 is located in front of a half- space $z < z_0$ of homogeneous material with no incident wave arriving from $z = -\infty$, then

$$
\Gamma(z_0) = 0 \qquad \text{(homogeneous half-space)}
\tag{23}
$$

For many situations, a combination of (21)- (23) may be used to arrive at a suitable "initial" condition $\Gamma(L) = \Gamma_0$ in order to render the solution to (19) unique.

7

Although the solution to (19) can be obtained numerically using standard ordinary differential equation solvers available in computer libraries, it was initially felt that a closed-form approximate solution would be desirable in order to speed up computations and to make design easier. To that end, we investigated several types of such approximations which can be found in the literature. The most common one is similar to a WKB expression and which we denote the *phase-integral approximation*. It is obtained [11],[12] by assuming that the reflection coefficient $\Gamma(z)$ is sufficiently small in magnitude that Γ^2 can be neglected compared to 1 in (19). Thus, (19) becomes approximately

$$\Gamma'(z) = 2\hat{\gamma}(z) - \hat{N}(z) \tag{24}$$

which is a first-order *linear* equation whose solution is written exactly as:

$$\Gamma_{ph}(z) = e^{-2\int_z^L \hat{\gamma}(z')\,dz'}\{\Gamma(L) + \int_z^L \hat{N}(z')e^{2\int_{z'}^L \hat{\gamma}(z'')\,dz''}\,dz'\} \tag{25}$$

and in particular

$$\Gamma_{ph}(0) = e^{-2\int_0^L \hat{\gamma}(z')\,dz'}\Gamma(L) + \int_0^L \hat{N}(z')e^{-2\int_0^{z'} \hat{\gamma}(z'')\,dz''}\,dz' \tag{26}$$

Note that in this approximation the reflection coefficient is approximately the sum of

$$\Gamma_{ph1}(0) = e^{-2\int_0^L \hat{\gamma}(z')\,dz'}\Gamma(L) \tag{27}$$

which is the reflection coefficient at the back of the layer, transferred forward through the layer as if the characteristic impedance were constant (cf. eqn. (21)), and

$$\Gamma_{ph2}(0) = \int_0^L \hat{N}(z')e^{-2\int_0^{z'} \hat{\gamma}(z'')\,dz''}\,dz' \tag{28}$$

which is the reflection coefficient we would see from the inhomogeneous layer if $\Gamma(L) = 0$, i. e., if the layer were backed by a homogeneous absorber halfspace [10].

Gaydabura [14] has proposed a modification of the phase-integral approximation which is claimed to be more accurate because it eliminates the possibility that the modulus of the reflection coefficient might be greater than one. This approximation can be written in our notation as

$$\Gamma_G(0) = \tanh\{e^{-2\int_0^L \hat{\gamma}(z')\,dz'}\operatorname{arctanh}\Gamma(L) + \Gamma_{ph2}(0)\} \tag{29}$$

If the imaginary part of the curly brackets in (29) is less than $\pi/4$ in absolute value, then this approximation will indeed obey $|\Gamma_G(0)| < 1$. However, there is no guarantee that this will always occur.

8

Another way of modifying the approximation (26) was proposed by Frances-chetti (see [15],[16]). Here it is not $|\Gamma|^2$ which must be small compared to one, but only $|\Gamma_{ph2}|^2$. In this way, initial conditions where $|\Gamma(L)|$ is not small may still be accurately accommodated. In our notation, this approximation is

$$\Gamma_F(0) = \Gamma_{ph2}(0) + \frac{\Gamma_{ph1}(0)}{1 + \Gamma_{ph1}(0) \int_0^L \hat{N}(z') e^{2\int_0^{z'} \hat{\gamma}(z'') dz''} dz'} \tag{30}$$

It too must be checked numerically to assess its range of usefulness.

3 Comparison of the Approximate Formulas

In this section, we choose a specific model with which to assess the accuracy of the approximations (26) (29) and (30). For greater simplicity, we consider a perpendicularly polarized plane wave incident upon an array of linearly tapered wedges (Fig. 4),where

$$d(z)/a = z/L \tag{31}$$

and L is the total depth of the tapered region. Then by (9), (10) and (3), if the absorber is taken to be nonmagnetic ($\hat{\mu}_a = \mu_0$), we have

$$\hat{\epsilon}_{eff}(z) = \epsilon_0 \cos^2 \theta + (\epsilon_a - \epsilon_0)\frac{z}{L} \tag{32}$$

Thus,

$$\hat{\gamma}(z) = jk_0\sqrt{\cos^2 \theta + \hat{\Delta} z/L} \tag{33}$$

and

$$\hat{Z}_c(z) = \frac{Z_0}{\sqrt{\cos^2 \theta + \hat{\Delta} z/L}} \tag{34}$$

where $Z_0 = (\mu_0/\epsilon_0)^{1/2}$, and

$$\hat{\Delta} = \left(\frac{\hat{\epsilon}_a}{\epsilon_0} - 1\right) \tag{35}$$

To help in the evaluation of (26), (29) and (30), define

$$P(z) \equiv -2j \int_0^z \hat{\gamma}(z') dz' \tag{36}$$

so that in the present case

$$\begin{aligned}
P(z) &= 2k_0 \int_0^z \sqrt{\cos^2 \theta + \hat{\Delta} z'/L}\, dz' \\
&= \frac{4k_0 L}{3\hat{\Delta}} \left\{ [\cos^2 \theta + \hat{\Delta} z/L]^{3/2} - \cos^3 \theta \right\}
\end{aligned} \tag{37}$$

9

Then (27) can be written as

$$\Gamma_{ph1}(0) = e^{-jP(L)}\Gamma(L) \tag{38}$$

where

$$P(L) = \frac{4}{3}k_0 L \frac{(\cos^2\theta + \hat{\Delta}) + \cos\theta\sqrt{\cos^2\theta + \hat{\Delta}} + \cos^2\theta}{\sqrt{\cos^2\theta + \hat{\Delta}} + \cos\theta} \tag{39}$$

From (20) we can write

$$\hat{N}(z) = -\frac{\hat{\Delta}}{4L}\left[\cos^2\theta + \hat{\Delta}z/L\right]^{-1} \tag{40}$$

and so equation (28) can be written

$$\begin{aligned}
\Gamma_{ph2}(0) &= \int_0^L \hat{N}(z')e^{-jP(z')}\,dz' \\
&= -\frac{1}{6}\int_0^{P(L)} \frac{e^{-jP}\,dP}{P+P_0}
\end{aligned} \tag{41}$$

by changing variables from z' to P, where

$$P_0 = \frac{4k_0 L}{3\hat{\Delta}}\cos^3\theta \tag{42}$$

The integral in (41) can be expressed in terms of the exponential integral of complex argument [17]:

$$E_1(z) = \int_z^\infty \frac{e^{-t}}{t}dt \tag{43}$$

and takes the form

$$\Gamma_{ph2}(0) = \frac{1}{6}e^{jP_0}[E_1(jP_1) - E_1(jP_0)] \tag{44}$$

where

$$P_1 = P_0 + P(L) = \frac{4k_0 L}{3\hat{\Delta}}(\cos^2\theta + \hat{\Delta})^{3/2} \tag{45}$$

It remains to calculate the integral in (30), which is quite similar to (41):

$$\begin{aligned}
\int_0^L \hat{N}(z')e^{2\int_0^{z'}\hat{\gamma}(z'')\,dz''}\,dz' &= \int_0^L \hat{N}(z')e^{jP(z')}\,dz' \\
&= \frac{1}{6}e^{-jP_0}[E_1(-jP_1) - E_1(-jP_0)]
\end{aligned} \tag{46}$$

Using these results in (26), (29) and (30) gives

$$\Gamma_{ph}(0) = e^{-jP(L)}\Gamma(L) + \frac{1}{6}e^{jP_0}[E_1(jP_1) - E_1(jP_0)] \tag{47}$$

$$\Gamma_G(0) = \tanh\left\{e^{-jP(L)}\text{arctanh}\,\Gamma(L) + \frac{1}{6}e^{jP_0}[E_1(jP_1) - E_1(jP_0)]\right\} \tag{48}$$

$$\begin{aligned}
\Gamma_F(0) = &\frac{e^{-jP(L)}\Gamma(L)}{1 + \frac{1}{6}\Gamma(L)e^{-jP_1}[E_1(-jP_1) - E_1(-jP_0)]} \\
&+ \frac{1}{6}e^{jP_0}[E_1(jP_1) - E_1(jP_0)]
\end{aligned} \tag{49}$$

10

When we specialize to normal incidence ($\theta = 0$), equation (47) becomes identical to that obtained by Bucci and Franceschetti [10] for this case.

The bulk properties $\hat{\epsilon}_a = \epsilon_0(\epsilon'_r - j\epsilon''_r)$ have been measured experimentally over the frequency range of 30-300 MHz[1] for several commercially made types of graphite-impregnated foam absorbers. The results are displayed in Table 1, where it can be seen that substantially different values and variations of the real and imaginary parts of $\hat{\epsilon}_a$ may occur.

These values will be used in our numerical examples. Note in particular that (especially for the lower frequencies) $\hat{\epsilon}_a$ is such that $|\hat{\Delta}| >> 1$, and thus only $\Gamma(L)$ and P_0 can introduce significant dependence of (47)-(49) on the incidence angle θ, because

$$P_1 \simeq P(L) \simeq \frac{4}{3}k_0 L \sqrt{\hat{\Delta}} \tag{50}$$

in this limit. As $\cos\theta \rightarrow 0$, $E_1(\pm jP_0) \rightarrow \infty$, and so these formulas will all become inaccurate at grazing incidence.

In the next section, we will compare the approximate results (47)-(49) for this case with exact values obtained from a solution of (19), (33) and (40). Although this exact solution can be written down in closed form using Airy functions [11], [18], [19], we will find it more convenient to use standard computer subroutines for the numerical solution of ordinary differential equations, since this is required for the analysis of more general geometries in any case.

4 Numerical Results

A standard Runge-Kutta algorithm [20] was used to solve the Riccati equation (19) subject to a given boundary condition $\Gamma(L)$ at $z = L$. For all cases studied here, the array of cones or wedges had a taper length of L, and a backing layer of homogeneous absorber of thickness d. Behind the backing layer there is assumed to be a perfectly conducting wall that serves to shield the measurement area (Fig. 6).

If calculations for many values of $\Gamma(L)$ are required, it is more efficient to calculate $\Gamma(0)$ for three different values of $\Gamma(L)$, and then to use the fact that any arbitrary solution of (19) can be expressed in terms of them [21]. In more physical terms, we can note [22] that the inhomogeneous layer can be represented as a two-port network with scattering matrix $[S]$, terminated at port 2 (the back plane of the layer) by a load whose reflection coefficient is $\Gamma(L)$—see Fig. 7. Then $\Gamma(0)$ is the reflection coefficient seen looking into port 1:

$$\Gamma(0) = \frac{(S_{12}S_{21} - S_{11}S_{22})\Gamma(L) + S_{11}}{1 - S_{22}\Gamma(L)} \equiv \frac{-d\Gamma(L) + S_{11}}{1 - S_{22}\Gamma(L)} \tag{51}$$

11

Table 1: Bulk properties of some commercial absorber samples.

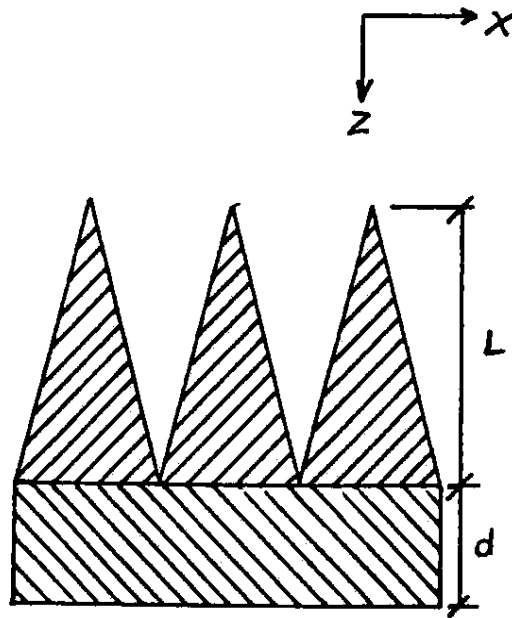| Frequency (MHz)	Sample I		Sample II		Sample III	
	ϵ_r'	ϵ_r''	ϵ_r'	ϵ_r''	ϵ_r'	ϵ_r''
30	7.9	2.5	9.2	7.6	16.6	9.3
35	7.6	2.5	8.4	7.3	15.5	9.3
40	7.4	2.6	7.8	7.1	14.5	9.3
45	7.2	2.6	7.2	6.8	13.8	9.1
50	7.0	2.6	6.8	6.5	12.9	8.9
60	6.7	2.6	6.0	6.0	11.8	8.6
70	6.3	2.6	5.5	5.6	11.0	8.2
80	6.0	2.6	5.0	5.3	10.1	7.9
90	5.8	2.6	4.6	5.0	9.5	7.6
100	5.8	2.6	4.3	4.7	9.1	7.3
125	5.5	2.5	3.8	4.2	8.1	6.7
150	5.3	2.5	3.6	3.8	7.4	6.1
175	5.0	2.4	3.3	3.4	6.9	5.6
200	4.8	2.4	3.1	3.2	6.5	5.2
250	4.6	2.4	2.8	2.8	6.2	4.7
300	4.4	2.5	2.6	2.6	6.0	4.5

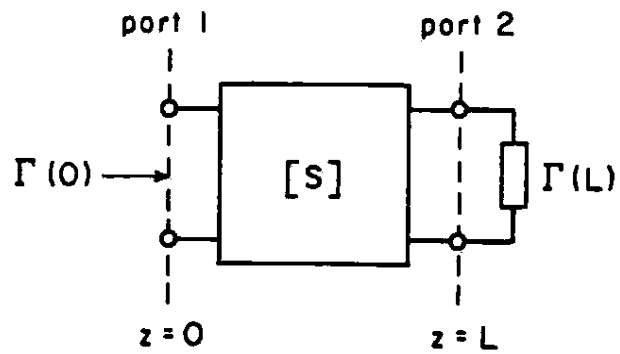Figure 6: Geometry of wedge and cone tapers.

Figure 7: Equivalent two-port network for the inhomogeneous absorbing layer.

13

where

$$d = S_{11}S_{22} - S_{12}S_{21} \tag{52}$$

is the determinant of $[S]$.

If Γ_s, Γ_0 and Γ_m represent the values of $\Gamma(0)$ obtained for short-circuit ($\Gamma(L) = -1$), open-circuit ($\Gamma(L) = +1$) and matched ($\Gamma(L) = 0$) loads respectively, then

$$\Gamma_s = \frac{d + S_{11}}{1 + S_{22}}$$

$$\Gamma_0 = \frac{-d + S_{11}}{1 - S_{22}}$$

$$\Gamma_m = S_{11}$$

and these may be solved to give

$$\left. \begin{array}{rcl} S_{11} & = & \Gamma_m \\ S_{22} & = & \frac{2\Gamma_m - \Gamma_s - \Gamma_0}{\Gamma_s - \Gamma_0} \\ d & = & \frac{\Gamma_m(\Gamma_s + \Gamma_0) - 2\Gamma_s\Gamma_0}{\Gamma_s - \Gamma_0} \end{array} \right\} \tag{53}$$

It might be noted by comparison with (30) that Franceschetti's approximation is equivalent to the following approximations to the S-parameters:

$$S_{11} = \Gamma_{ph2}(0) = \int_0^L \hat{N}(z')e^{-2\int_0^{z'} \hat{\gamma}(z'')\,dz''}\,dz' \tag{54}$$

$$S_{22} = -\int_0^L \hat{N}(z')e^{-2\int_{z'}^L \hat{\gamma}(z'')\,dz''}\,dz' \tag{55}$$

$$S_{12}S_{21} = e^{-2\int_0^L \hat{\gamma}(z')\,dz'} \tag{56}$$

For an array of wedges, we may have the wedge edges parallel either to the x-axis or y-axis, and polarization of the incident plane wave electric field either perpendicular or parallel to the plane of incidence xz. For the perpendicular polarization, with the edges oriented along the y-axis, numerical results calculated from the Runge-Kutta solution of (19) are shown in Figure 8. This figure shows a graph of the magnitude of the reflection coefficient versus frequency corresponding to various thicknesses of homogeneous absorbent material behind the wedges. From the plot, it is evident that by varying the absorber thickness the response of the structure can be changed quite dramatically. It should be noted that this plot, as well as others that follow, were obtained assuming $\hat{\epsilon}_a$ to be that of Sample II in Table 1, unless otherwise stated.

From the plot, we see that the high frequency response is very good, however at the low frequency end, we see reflections of 40 to 50 percent. We also notice
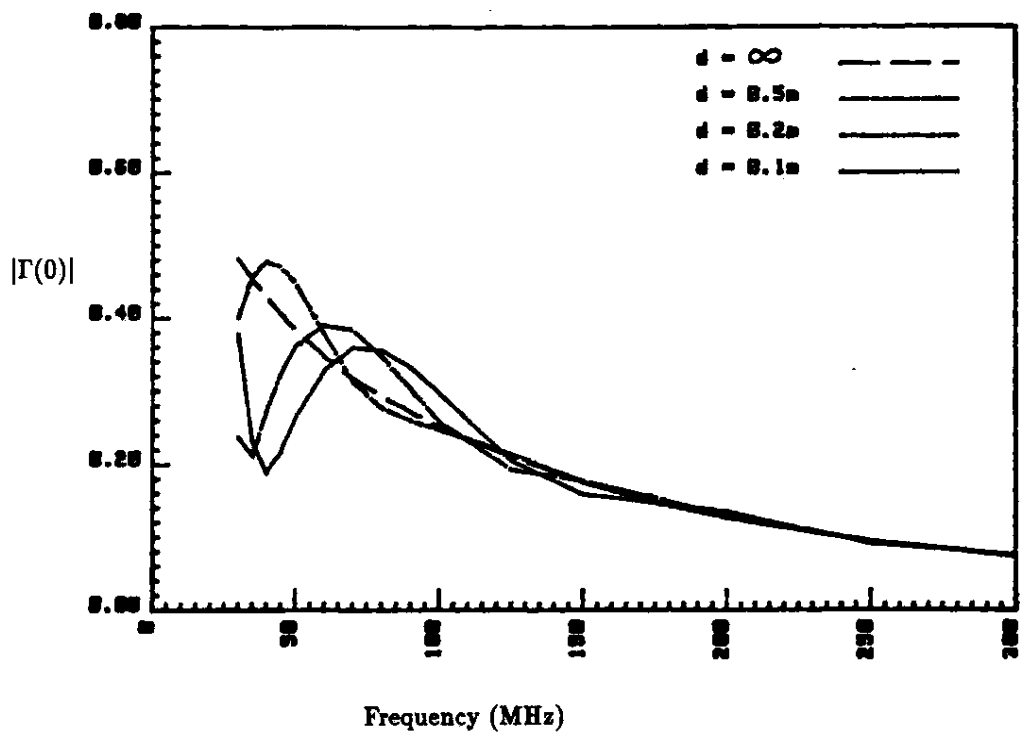
14

Figure 8: Magnitude of the reflection coefficient for perpendicular polarization with wedge edges oriented along the y-axis.

that by varying the absorber thickness (d), minima develop in the response curves which can be shifted by altering the dimension d.

These minima are a result of constructive and destructive interference that occurs because of multiple reflections within the wedges. The reflection coefficient (Γ) is lowered somewhat because of the various minima. However, Γ is lowered at the expense of peaks that also appear on the curves.

Figure 8 is a plot of the (numerically) "exact" solution, while Figures 9 and 10 show comparisons of the exact and the approximate values of $|\Gamma|$. From Figure 9, we see that the phase integral and Franceschetti approximations are virtually indistinguishable from one another except around 38 MHz, and for the most part, they are indistinguishable from the exact solution. We see that the Gaydabura approximation is the worst of these three approximations and does not match the exact solution well until around 90 MHz.

Figure 11 shows results for d equal to 0.1 m, for four different angles of incidence; $0°$, $30°$, $45°$, and $60°$. We see that as the angle of incidence in increased, the response curves increase in magnitude. This is consistent with known behavior of reflection coefficients at grazing angles, for which $|\Gamma|$ approaches 1.

Results for perpendicular polarization were also calculated from the Ricatti equation for the case of an array of pyramid cones of square cross-section. The length of the tapered section was taken to be 1 m, and the thickness of the backing absorber was varied from 0.1 m to ∞. Numerical results are shown in Figure 12. The reflection coefficient Γ is plotted for four different angles of incidence in Fig. 13: $0°$, $30°$, $45°$ and $60°$.

For the parallel polarization, numerical results are the same as for perpendicular polarization when the angle of incidence is equal to zero (see Figure 12). Plots for various angles of incidence are shown in Figure 14.

Some interesting observations can be made between the two different geometries. The cone geometry is more effective at higher frequencies, while the wedge geometry is more effective at the low frequency end. For both geometries, Γ can be altered quite dramatically by relatively minor variations in the backing absorber. This is made aparent by the shifts of the minima in the response curves.

We are now in a position to analyze the effect of material properties on the response of a wall of pyramid cones at frequencies from 30 to about 200 MHz. We analyzed two different size cones (6ft and 4ft) with material properties as measured from "off-the-shelf" cone absorbers from a well-known manufacturer to determine which would have the best response. The material parameters are shown in Table 2.

The results are shown in Figure 15. The results that were obtained are just the opposite of what one might have expected: the 4 ft cones generally outperformed the 6ft cones.

This can be explained by noting from Table 2 that the 4ft cones are doped more heavily (the real and imaginary parts of $\hat{\epsilon}_a$ are larger) than the 6ft cones. Absorber manufacturers make cones in this way to achieve best performance at
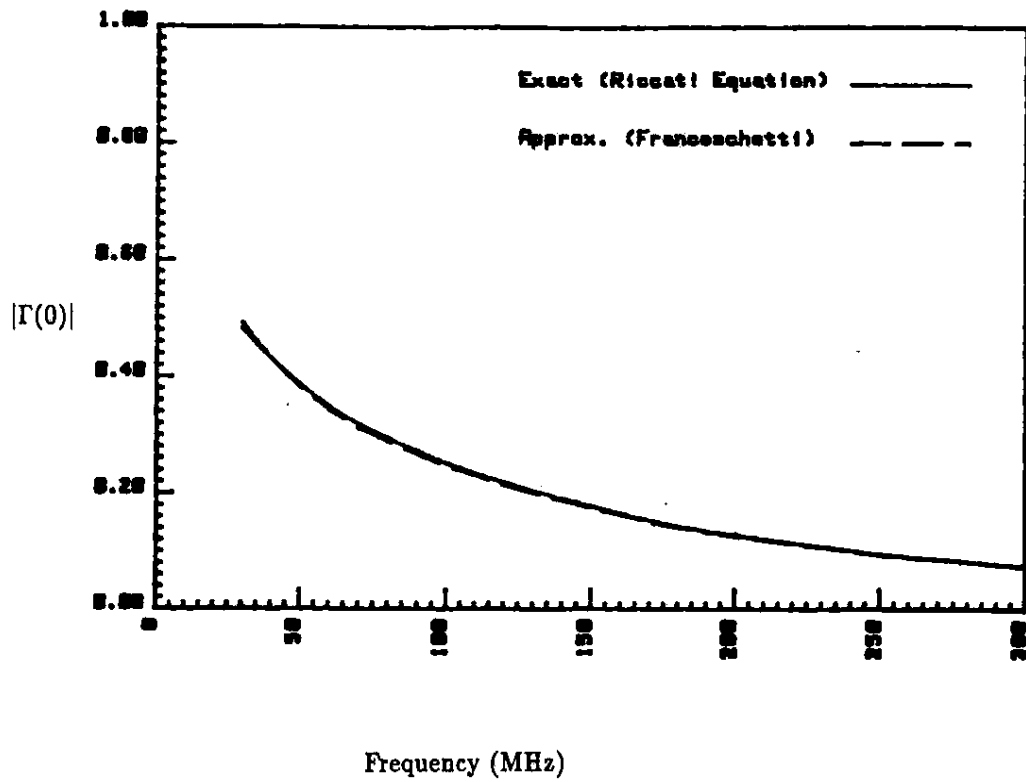
16

.

Figure 9: Exact and approximate reflection coefficients for a wedge array with an infinite backing layer (perpendicular polarization; wedge edges oriented along the y-axis).
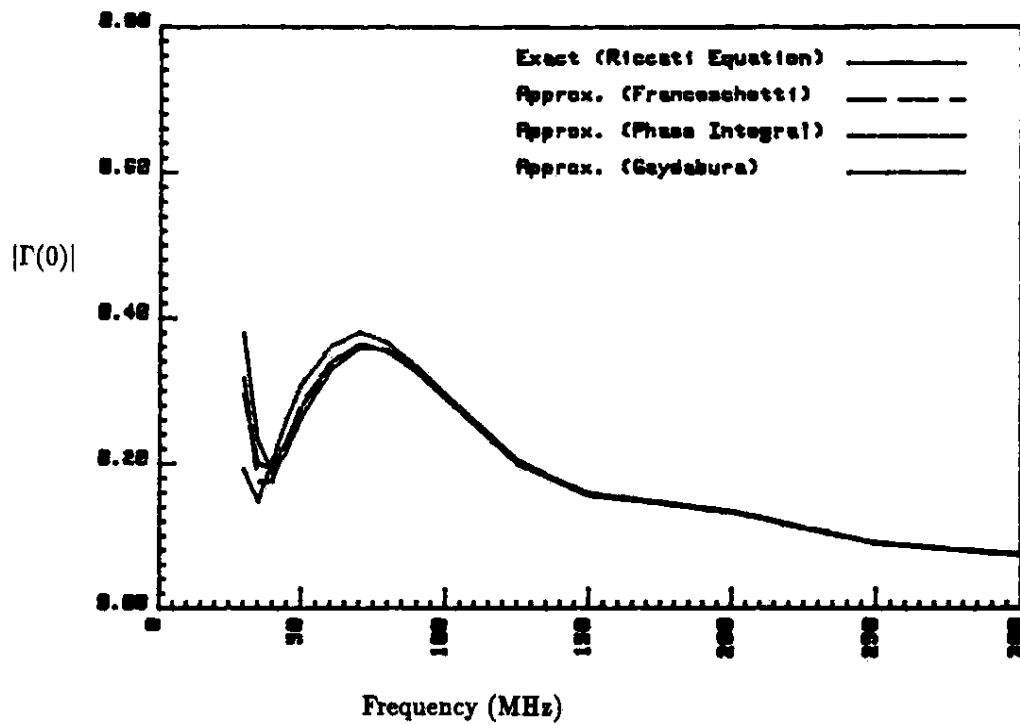
17

Figure 10: Exact and approximate reflection coefficients for a wedge array with a 0.1m backing layer (perpendicular polarization; wedge edges oriented along the y-axis).
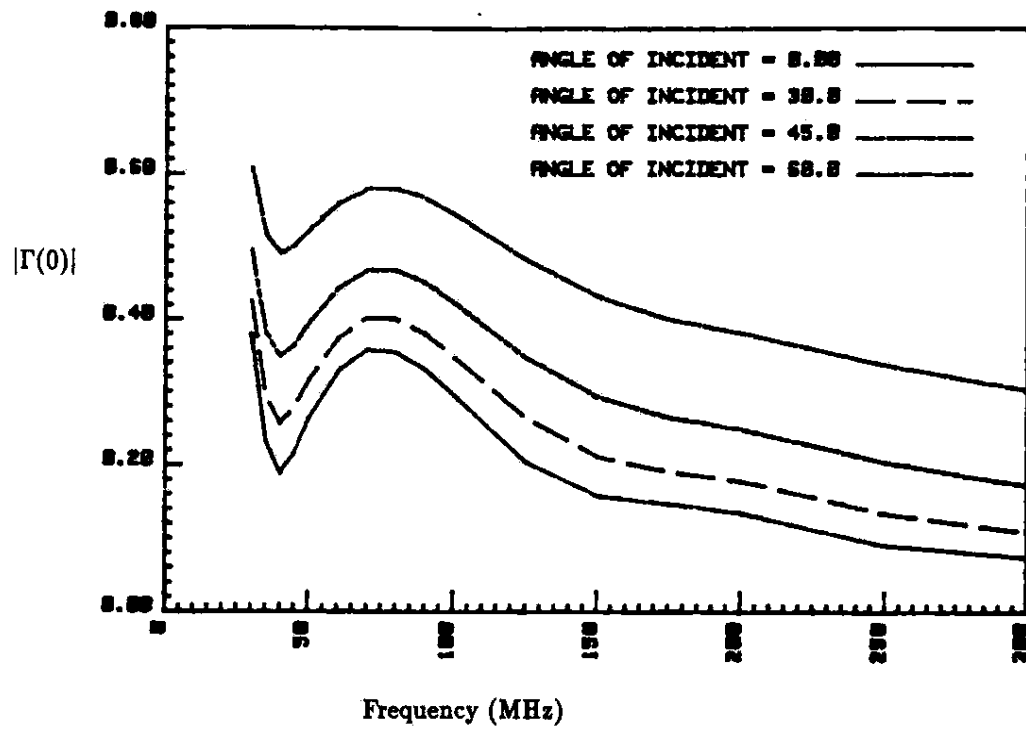
18

Figure 11: Reflection coefficient of perpendicularly polarized waves at various angles of incidence when the wedge edges are oriented along the y-axis.
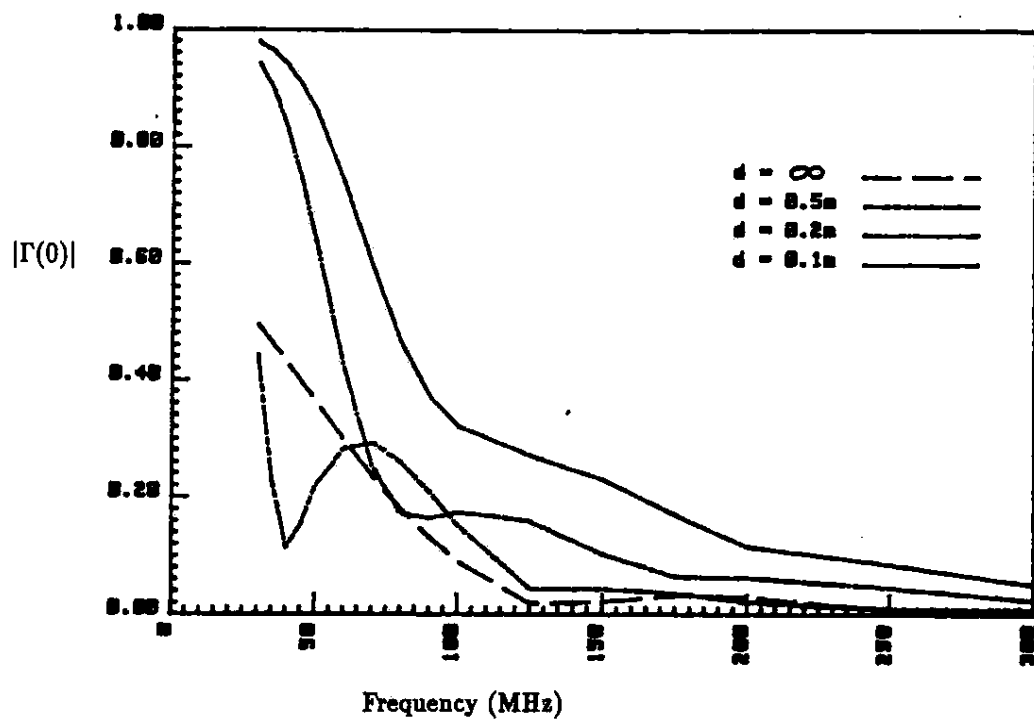
Figure 12: Perpendicular polarization reflection coefficient for pyramid cone array.
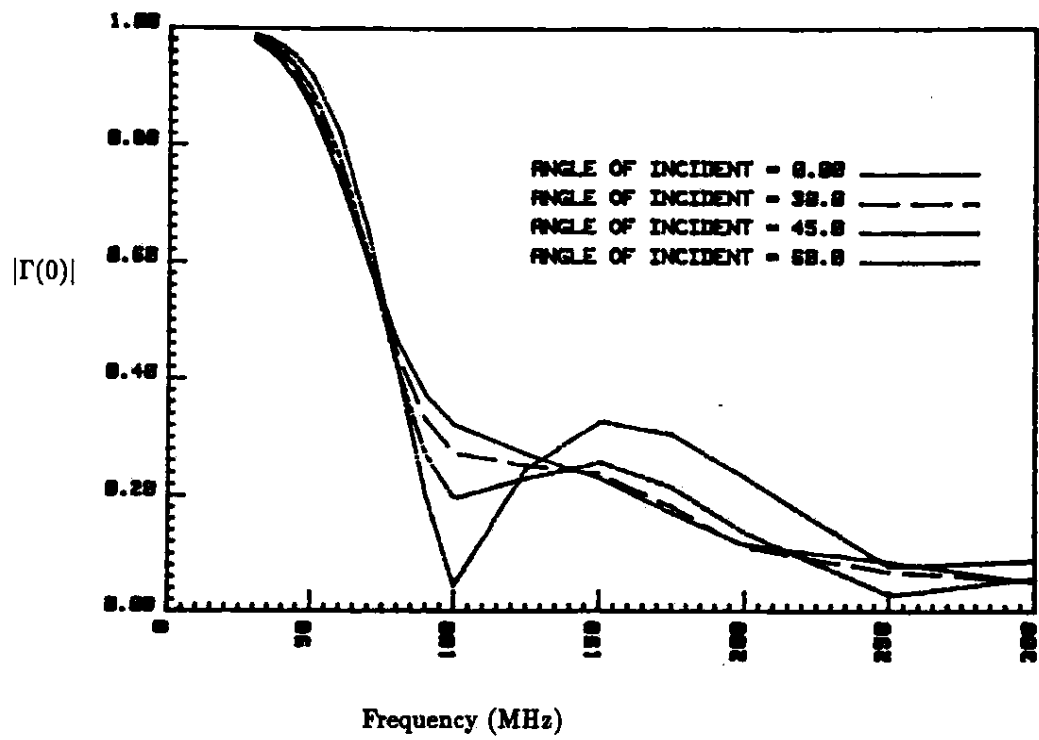
Figure 13: Reflection coefficient versus incidence angle for pyramid cone array (perpendicular polarization).
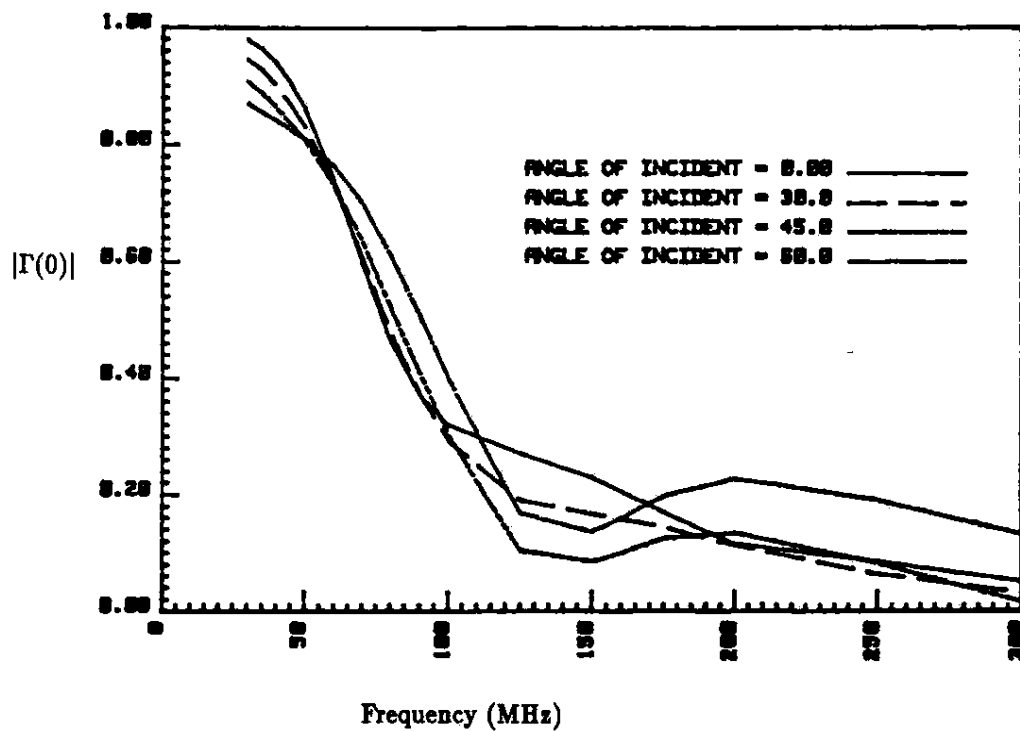
Figure 14: Reflection coefficient versus incidence angle for pyramid cone array (parallel polarization).

Table 2: Measured bulk material properties for 6ft and 4ft "off-the-shelf" absorber.

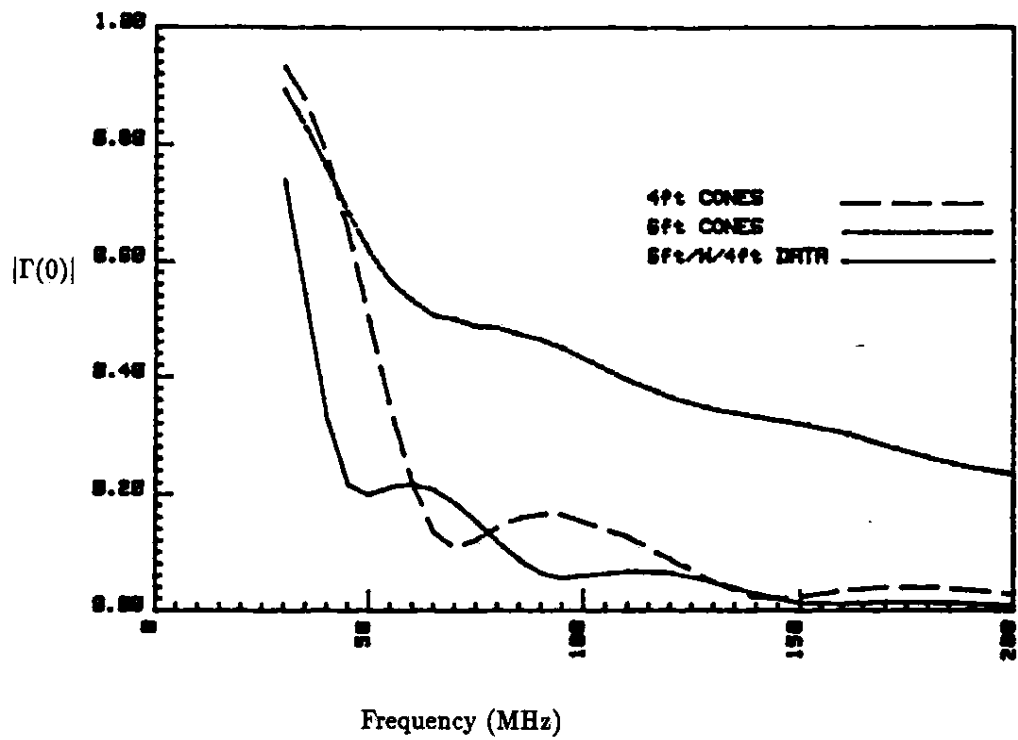| Frequency (MHz)	6ft cones		4ft cones	
	ϵ_r'	ϵ_r''	ϵ_r'	ϵ_r''
30	4.41	2.24	15.21	10.22
35	4.23	2.11	13.94	10.03
40	4.11	1.95	12.97	9.87
45	3.98	1.84	12.08	9.66
50	3.89	1.75	11.30	9.49
55	3.83	1.68	10.68	9.35
60	3.74	1.60	10.08	9.17
65	3.70	1.57	9.55	9.03
70	3.66	1.50	9.09	8.90
75	3.61	1.47	8.65	8.78
80	3.58	1.41	8.27	8.66
85	3.56	1.38	7.90	8.59
90	3.52	1.34	7.55	8.44
95	3.49	1.31	7.24	8.37
100	3.47	1.29	6.93	8.29
120	3.40	1.21	5.84	7.98
140	3.37	1.16	4.92	7.79
160	3.36	1.13	4.10	7.61
180	3.37	1.22	3.31	7.44
200	3.39	1.23	2.55	7.21

Figure 15: Reflection coefficients of "off-the-shelf" 6ft and 4ft cones, and of 6ft cones made of modified material.

higher frequencies. As the cones get larger in size, they require less doping to obtain the same high frequency response as small cones.

After analyzing the properties of the two different cones, the question was raised: what if we made a 6ft cone whose material properties were the same as "off-the-shelf" 4ft cones? This particular configuration was analyzed and the results are also shown in Figure 15. We see that the new cone performs substantially better than either of the stock (6ft or 4ft) cones.

A second approach to improving the response of the pyramid-cone structure at low frequencies is to alter the length L of the tapered section and the thickness d of the backing layer (Fig. 6). Suppose that we wish to maintain the overall thickness $L + d$ of the absorber structure a constant (6 feet, in the example we look at below). Then, we can still vary L (hence also d) individually to see the effect on the overall frequency behavior of the reflection coefficient. Figure 16 illustrates how the response changes when the dimensions are varied (the modified material parameters—those of the 4 foot cones from Table 2—are used here). From the figure we see that the best response is obtained when $L = 1.22$ m and $d = 0.6$ m, making the tapered section occupy about 67 percent of the total cone length. A standard 6ft cone has a tapered section of 1.57 m and a backing layer of 0.25 m.

The results for the optimized design were then compared with those for the standard 6ft geometry, and are shown in Figure 17. From the plot we see that the new design performs substantially better than does the original cone. The original cone reflects 50 percent of the energy at 30 MHz, where the new design reflects only about 10 percent at 30 MHz.

Such improved-design cones have been made and installed in anechoic chambers at two IBM manufacturing sites. Results of measurements made in those chambers and comparisons with theoretical models for the chambers will be reported in a separate publication.

5   Conclusion

There are two approximations inherent in our analysis which may limit its range of validity. The first is our use of the continuum model (1)-(5) to account for the anisotropic effect of the wedge or pyramid shapes. These expressions are strictly valid only in the low-frequency limit, and begin to deteriorate if the taper of the absorber is too fast (wedge angle greater than 20°) or the period dimension of the wedges or cones is greater than about 10% or 20% of a free space wavelength. If we can introduce frequency-dependent correction terms to the expressions for $[\bar{\epsilon}]$ and $[\bar{\mu}]$ as suggested in [10] and [23], it should prove possible to relax these limitations substantially.

More fundamental in nature is the underlying assumption that only a single, quasi-plane wave field exists in the tapered absorber, allowing the concept of the equivalent tensor parameters to make sense at all. If frequency becomes high
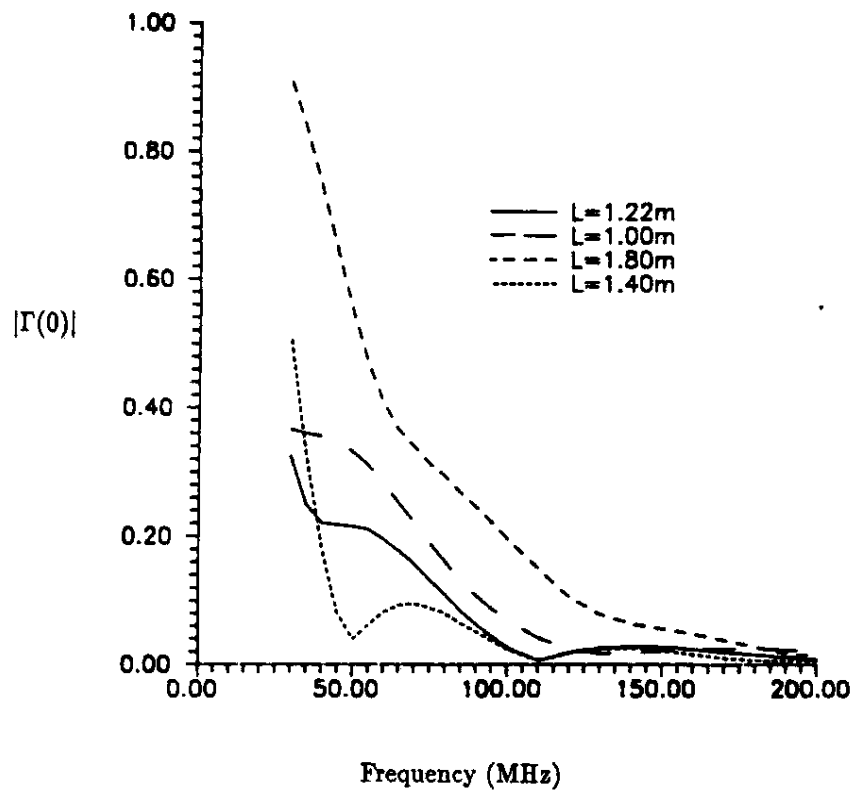
25

Figure 16: Effect of varying taper length L for 6 foot cone absorbers.
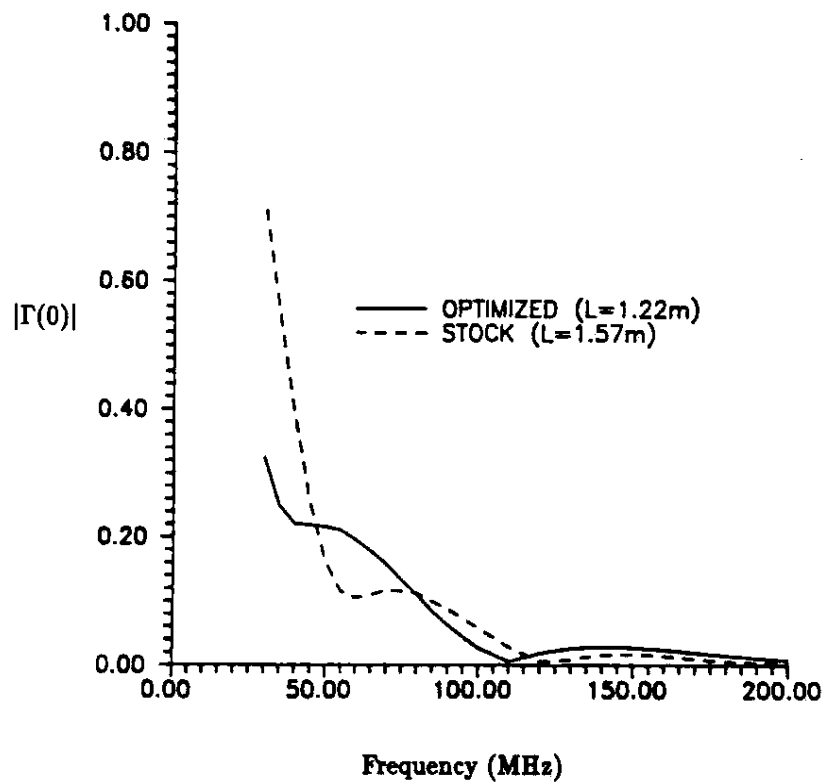
Figure 17: Comparison of standard and optimally tapered 6 foot cone reflection coefficients.

enough, higher-order Floquet modes may begin to propagate in the structure [24]. Although the theory of [24] is not presently well enough developed to account adequately for the presence of these modes, numerical evidence for an equivalent waveguide model [23] suggests that the period of the wedges or cones might become as large as a half wavelength before higher-order modes need to be taken into account. Further work needs to be done on both of these points.

The numerical results presented here have shown the possibility of dramatically improving the low-frequency reflection properties of pyramid-cone absorber. This may be at the expense of higher frequency response, but this range is usually so good that it could be acceptable to trade a little performance here for the great improvement at the low end. Other attempts at improved absorber design will be investigated in future work.

A Properties of the Reflection Coefficient in a Lossy Layer

In this appendix we will derive a few elementary properties of $Z(z)$ and $\Gamma(z)$ in a lossy layer as defined by eqns. (15) and (18). For the plane waves described by eqns. (8), Poynting's theorem in its complex differential form is

$$\frac{d}{dz}[E(z)H^*(z)] = j\omega[\hat{\epsilon}^*_{eff}(z)|E(z)|^2 - \hat{\mu}_{eff}(z)|H(z)|^2] \tag{57}$$

where * denotes complex conjugate. Suppose that the plane $z = z_0$ is a perfect conductor so that $E(z_0) = 0$. Then integrating (57) from z ($< z_0$) to z_0 gives

$$
\begin{aligned}
E(z)H^*(z) &= Z(z)|H(z)|^2 \\
&= -j\omega \int_z^{z_0} [\hat{\epsilon}^*_{eff}(z')|E(z')|^2 - \hat{\mu}_{eff}(z')|H(z')|^2]\,dz' \tag{58}
\end{aligned}
$$

Taking the real part of both sides and writing $\hat{\epsilon}_{eff} = \epsilon'_{eff} - j\epsilon''_{eff}$, $\hat{\mu}_{eff} = \mu'_{eff} - j\mu''_{eff}$, with $\epsilon''_{eff}, \mu''_{eff} \geq 0$, we have the relation expressing conservation of time-average energy as:

$$
\begin{aligned}
\text{Re}[Z(z)] &= \frac{\omega}{|H(z)|^2} \int_z^{z_0} [\epsilon''_{eff}(z')|E(z')|^2 + \mu''_{eff}(z')|H(z')|^2]\,dz' \\
&\geq 0 \tag{59}
\end{aligned}
$$

Thus, when no sources exist between a perfect conductor (which may be removed to $z_0 \to \infty$ if desired) and an observation point z, the impedance $Z(z)$ is a purely passive impedance, lying in the right half of the complex Z-plane.

If $\hat{Z}_c$ is purely real, it is well known that (18) and (59) imply that Γ lies within the unit circle of the complex Γ-plane: $|\Gamma| \leq 1$. However, if $\hat{Z}_c$ is complex, this

is no longer the case [25]-[27]. Let us write $\hat{Z}_c$ in terms of its magnitude and phase:

$$\hat{Z}_c = Z_c e^{j\phi} \tag{60}$$

where

$$Z_c = \left(\frac{\mu'^2_{eff} + \mu''^2_{eff}}{\epsilon'^2_{eff} + \epsilon''^2_{eff}}\right)^{1/4} \tag{61}$$

and

$$\phi = \frac{1}{2}\left[\tan^{-1}\left(\frac{\epsilon''_{eff}}{\epsilon'_{eff}}\right) - \tan^{-1}\left(\frac{\mu''_{eff}}{\mu'_{eff}}\right)\right] \tag{62}$$

Note that $|\phi| < \pi/4$ if $\hat{\epsilon}_{eff}$ and $\hat{\mu}_{eff}$ are given by (10) or (12).

Now from (18) and (60),

$$\begin{aligned}
\frac{Z(z)}{Z_c(z)}e^{-j\phi(z)} &= \frac{1 + \Gamma(z)}{1 - \Gamma(z)} \\
&= \frac{1 - \Gamma_r^2(z) - \Gamma_i^2(z) + 2j\Gamma_i(z)}{[1 - \Gamma_r(z)]^2 + \Gamma_i^2(z)}
\end{aligned} \tag{63}$$

where $\Gamma(z) \equiv \Gamma_r(z) + j\Gamma_i(z)$ where Γ_r and Γ_i are real. But if, by (59), $\text{Re}[Z(z)] \geq 0$, then (63) implies

$$[1 - \Gamma_r^2 - \Gamma_i^2]\cos\phi - 2\Gamma_i \sin\phi \geq 0 \tag{64}$$

or,

$$|\Gamma(z) + j\tan\phi(z)| \leq \sec\phi(z) \tag{65}$$

Eqn. (65) describes the interior of a circle in the complex Γ-plane centered at $-j\tan\phi(z)$ and of radius $\sec\phi(z)$. When $\phi = 0$, this reduces to the unit circle as expected. If $\phi = \pm\pi/4$, then the circle attains its maximum radius of $\sqrt{2}$, and is centered at $\mp j$. Evidently, we may have $|\Gamma| > 1$ in appropriate circumstances if $\phi \neq 0$.

References

[1] R. E. Hiatt, E. F. Knott and T. B. A. Senior, "A study of VHF absorbers and anechoic rooms," Technical Rept. 5391-1-F, Radiation Laboratory, Department of Electrical and Computer Engineering, University of Michigan, Ann Arbor, 1963.

[2] W. H. Emerson, "Electromagnetic wave absorbers and anechoic chambers through the years," *IEEE Trans. Ant. Prop.*, vol. 21, pp. 484-490 (1973).

[3] M. Yu. Mitsmakher and V. A. Torgovanov, *Bezekhovye Kamery SVCh.* Moscow: Radio i Svyaz', 1982.

29

[4] E. F. Knott, J. F. Shaeffer and M. T. Tuley, *Radar Cross Section*. Norwood, MA: Artech House, 1985, chapter 13.

[5] E. F. Kuester, "Low-frequency properties of transversely periodic lossy waveguides," *Sci. Rept. No. 92*, Electromagnetics Laboratory, Dept. of Electrical and Computer Engineering, University of Colorado, Boulder, 1987.

[6] O. Wiener, "Lamellare Doppelbrechung," *Physikal. Zeits.*, vol. 5, pp. 332-338 (1904).

[7] H.-G. Haddenhorst, "Durchgang von elektromagnetischen Wellen durch inhomogene Schichten," *Zeits. Angew. Physik*, vol. 7, pp. 487-496 (1955).

[8] S. M. Rytov, "Electromagnetic properties of a finely stratified medium"[Russian], *Zh. Exp. Teor. Fiz.*, vol. 29, pp. 605-616 (1955) [Engl. transl. in *Sov. Phys. JETP*, vol. 2, pp. 466-475 (1956)].

[9] R. Pottel, "Absorption elektromagnetischer Zentimeterwellen in künstlich anisotropen Medien," *Zeits. Angew. Physik*, vol. 10, pp. 8-16 (1958).

[10] O. M. Bucci and G. Franceschetti, "Scattering from wedge-tapered absorbers," *IEEE Trans. Ant. Prop.*, vol. 19, pp. 96-104 (1971).

[11] L. M. Brekhovskikh, *Waves in Layered Media*. New York: Academic Press, 1960, pp. 79-86, 215-233.

[12] R. E. Collin, *Foundations for Microwave Engineering*. New York: McGraw-Hill, 1966, pp. 251-254.

[13] K. Walther, "Reflection factor of gradual transition absorbers for electromagnetic and acoustic waves," *IRE Trans. Ant. Prop.*, vol. 8, pp. 608-621 (1960).

[14] I. S. Gaydabura, "A method for linearization of the equation of an inhomogeneous line"[Russian], *Radiotekh. Elektron.*, vol. 16, pp. 1805-1807 (1971) [Engl. transl. in *Radio Eng. Electron. Phys.*, vol. 16, pp. 1625-1627 (1971)].

[15] G. Latmiral, G. Franceschetti and R. Vinciguerra, "Analysis and synthesis of nonuniform transmission lines or stratified layers," *J. Res. NBS pt. D (Radio Prop.)*, vol. 67D, pp. 331-345 (1963).

[16] G. Franceschetti, "Scattering from plane layered media," *IEEE Trans. Ant. Prop.*, vol. 12, pp. 754-763 (1964).

[17] M. Abramowitz and I. A. Stegun, eds., *Handbook of Mathematical Functions*. Washington, DC: US Government Printing Office, 1964, chapter 5.

[18] S. Kozaki, S. Makino and Y. Mushiake, "Radio wave propagation in a medium having tapered conductivity," *Repts. Res. Inst. Elec. Commun. Tohoku Univ.*, vol. 21, pp. 72-83 (1969).

[19] P. Baldwin, "Some analytic solutions for a simple model of a microwave absorber," *Wave Motion*, vol. 1, pp. 215-223 (1979).

[20] A. H. Stroud, *Numerical Quadrature and Solution of Ordinary Differential Equations*. New York: Springer-Verlag, 1974.

[21] E. L. Ince, *Ordinary Differential Equations*. New York: Dover, 1956, pp. 23-25.

[22] D. M. Kerns and R. W. Beatty, *Basic Theory of Waveguide Junctions and Introductory Microwave Network Analysis*. Oxford: Pergamon Press, 1967, p. 88.

[23] V. I. Ponomarenko and I. P. Stadnik, "Calculation of the reflection coefficient of an electromagnetic wave from wedge-shaped radio-absorbing structures"[Russian], *Izv. VUZ Elektromekhanika*, no. 4, pp. 9-15 (1986).

[24] E. F. Kuester, "The fundamental properties of transversely periodic lossy waveguides," *Sci. Rept. No. 86*, Electromagnetics Laboratory, Dept. of Electrical and Computer Engineering, University of Colorado, Boulder, 1986.

[25] R. W. P. King, *Transmission-Line Theory*. New York: Dover, 1965, pp. 128-130, 251-254.

[26] R. J. Vernon and S. R. Seshadri, "Reflection coefficient and reflected power on a lossy transmission line," *Proc. IEEE*, vol. 57, pp. 101-102 (1969).

[27] J. Kretzschmar and D. Schoonaert, "Smith chart for lossy transmission lines," *Proc. IEEE*, vol. 57, pp. 1658-1660 (1969).